Available online at www.sciencedirect.com
SCIENCE DIRECT
Journal of Magnetic Resonance 181 (2006) 310–315
JMR Journal of Magnetic Resonance
www.elsevier.com/locate/jmr

Two-dimensional one pulse MAS of half-integer quadrupolar nuclei

Dominique Massiot [a], Julian Hiet [a], Nadia Pellerin [a], Franck Fayon [a], Michael Deschamps [a], Stefan Steuernagel [b], Philip J. Grandinetti [c,*]

[a] CRMHT-CNRS, UPR4212, 45071 Orléans cedex 2, France
[b] Bruker-Biospin GMBH, 76287 Rheinstetten, Germany
[c] Department of Chemistry, The Ohio State University, 120 W. 18th Avenue, Columbus, OH 43210-1173, USA

Received 3 April 2006
Available online 30 June 2006

Abstract

We show that the two-dimensional one pulse (TOP) representation of magic-angle spinning nuclear magnetic resonance data of half-integer quadrupolar nuclei has significant advantages over the conventional one-dimensional spectrum. The TOP spectrum, which correlates NMR frequency to spinning sideband order, provides a rapid determination of the number of sites as well as the size of the their quadrupolar coupling. Additionally, synchronous acquisition spectra of the central and satellite transition resonances can be separated by different projections of the TOP spectrum, with higher resolution spectra often found in the satellite transitions projection. A previously perceived problem of centerband aliasing in TOP can be eliminated with an algorithm that uses larger subspectral widths and the sideband order dimension to distinguish centerbands from sidebands.

Keywords: Solid-state NMR; Half-integer quadrupolar nuclei; Spinning sidebands

1. Introduction

Magic-angle spinning (MAS) improves resolution in solid-state NMR by averaging away frequency anisotropy. Under MAS, a broad anisotropic resonance is broken up into a centerband flanked by sidebands at multiples of the rotor frequency. At high MAS speeds only the centerband survives. At lower speeds, the sideband intensities can be analyzed to retrieve information about the anisotropy of the interactions [1] (e.g., chemical shift anisotropy, quadrupolar coupling) which provide further sample structure characterization. Several years ago, Blümich and coworkers [2,3] proposed the two-dimensional one pulse (TOP) MAS method where a ID MAS spectrum is mapped into a 2D spectrum correlating frequency and spinning sideband order. The experimental simplicity of TOP makes it a compelling method, and it is surprising that TOP has not been more widely utilized [4]. A limitation of TOP, however, is the spectral width in the frequency dimension is limited to integer divisors of the rotor frequency, and this cannot be easily corrected by increasing the rotor frequency since it also reduces the information content in the sideband intensities. Here, we show that TOP applied to half-integer quadrupolar nuclei, with minor modification, does not suffer as greatly from this limitation, and has other advantages that significantly increase the power of this overlooked approach. Additionally, since the TOP experiment only requires a single pulse, it is ideal for satellite transitions of quadrupolar nuclei, where rf fields strengths are often too weak to generate the kind of broadband π pulse excitation needed for the more sophisticated sideband manipulation experiments like PASS [5].

2. Theoretical background

A multipole expansion of the NMR frequency as a function of time during magic-angle spinning can be separated into non-rotor and rotor modulated components:

* Corresponding author. Fax: +1 614 292 1685.
E-mail address: grandinetti.l@osu.edu (P.J. Grandinetti).

1090-7807/$ - see front matter © 2006 Published by Elsevier Inc.
doi:10.1016/j.jmr.2006.05.007

$$\Omega(t,\phi_0) = \sum_{l=0} \omega_{l,0} + \sum_{l>0} \sum_{m\neq 0} \omega_{l,m} e^{im(\Omega_R t+\phi_0)},$$

where ϕ_0 is the initial rotor phase, Ω_R is the rotor speed, the index m runs from $-l$ to l, and l typically runs from zero to two for spin 1/2 nuclei and zero to four for half-integer quadrupolar nuclei experiencing second-order quadrupolar broadenings. In a one pulse NMR experiment the signal phase as function of t is

$$\Phi(t) = \int_0^t \Omega(s)\,ds = W_0 t - \sum_{l,m\neq 0} iW_{l,m}[e^{im(\Omega_R t+\phi_0)} - e^{im\phi_0}],$$

where we have defined

$$W_0 = \sum_{l=0} \omega_{l,0} \quad \text{and} \quad W_{l,m} = \frac{\omega_{l,m}}{m\Omega_R}.$$

Here, W_0 is the non-rotor modulated frequency, which will be orientation dependent for quadrupolar nuclei broadened to second-order or higher.

Following a derivation found in various NMR texts [6], the signal of a polycrystalline sample undergoing magic-angle spinning can be shown to have the form

$$S(t) = \sum_{N_0=-\infty}^{\infty} I_{N_0} e^{iW_0 t} e^{iN_0\Omega_R t} e^{-t/T_2}. \quad (1)$$

2.1. Time domain approach

The 1D time domain signal can be mapped into an intermediate 2D coordinate system with variables k and Ξ, as shown in Fig. 1, by defining

$$t = (\Xi/2\pi + k)t_R,$$

where $t_R = 2\pi/\Omega_R$ and k is an integer. In TOP, a more restricted mapping, with

$$\Xi = \Omega_R t \ (\mathbf{mod}\ 2\pi) \quad \text{and} \quad k = \left\lfloor \frac{t}{t_R} \right\rfloor,$$

where $\lfloor x \rfloor$ represents the integer part or floor function of x, is used to extract the 2D data-subset, indicated by the dots inside the dashed lines in Fig. 1B. The 2D signal in the k–Ξ coordinate system is

$$S(k,\Xi) = \sum_{N_0=-\infty}^{\infty} I_{N_0} e^{(iW_0 - 1/T_2)(\Xi/2\pi+k)t_R} e^{iN_0\Xi}.$$

From this expression one sees that the frequency and sideband order evolution are mixed in the Ξ coordinate. However, by applying the shearing (coordinate) transformation

$$\begin{pmatrix} t_1 \\ \Theta \end{pmatrix} = \begin{pmatrix} t_R & t_R/2\pi \\ 0 & 1 \end{pmatrix} \begin{pmatrix} k \\ \Xi \end{pmatrix}, \quad (2)$$

the signal is moved into a coordinate system of time and rotor pitch, given by

$$S(t_1,\Theta) = \sum_{N_0=-\infty}^{\infty} I_{N_0} e^{iW_0 t_1} e^{iN_0\Theta} e^{-t_1/T_2}, \quad (3)$$

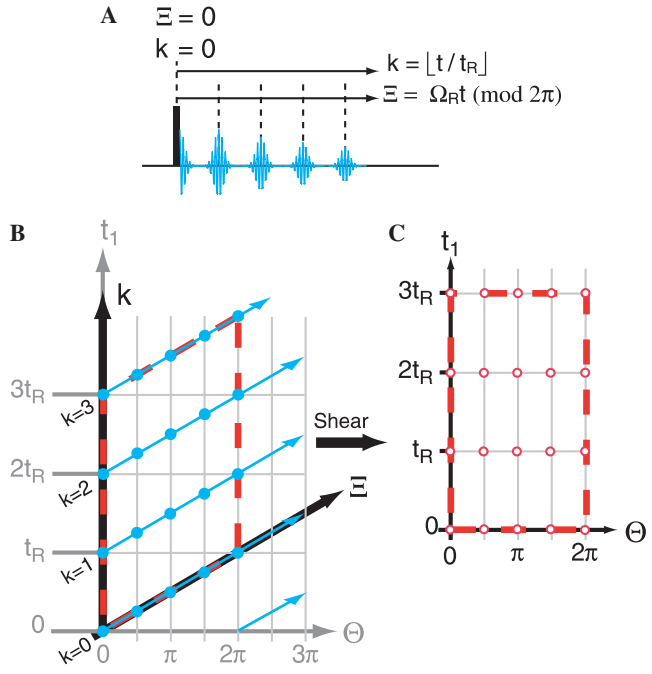

Fig. 1. (A) One pulse sample spinning experiment with coordinate definitions and timings. (B) Sampling trajectory (blue lines) of one pulse sample spinning data in the 2D t–Θ and k–Ξ coordinate systems. The slope of the sampling trajectory in the t–Θ coordinate system is the inverse rotor frequency. Identical data sets run parallel in the 2D plane and are separated by t_R and 2π, respectively, t–Θ coordinate system. (C) Sheared 2D data set that correlates time and rotor pitch.

and as shown in Fig. 1C. The 2D Fourier transform of Eq. (3) gives the 2D spectrum correlating frequency with spinning sideband order,

$$S(\omega_1, N) = I_N \mathcal{L}(\omega_1 - W_0), \quad (4)$$

where $\mathcal{L}(\omega)$ represents the lineshape of a single resonance.

We note that the spectral width limitation in the isotropic dimension of TOP could be overcome by employing well-known strategies for shifting the rotor pitch and isotropic time origins away from each other [5]. In such strategies the signal trajectories with different isotropic evolution time and rotor pitch origins are interleaved onto the sampling grid in Fig. 1 to obtain a two-dimensional spectrum with arbitrary isotropic dimension spectral width. For example, in the 2D-PASS experiment of Levitt and co-workers [7] a 5π pulse sequence is used to vary the rotor pitch while keeping isotropic evolution time constant. Conversely, in the FIREMAT experiment of Grant and coworkers [8], a 5π pulse sequence is used to vary the isotropic evolution time while keeping the rotor pitch constant.

2.2. Frequency domain approach

The ID spectrum obtained from the Fourier transform of Eq. (1) is

$$S(\omega) = \sum_{N_0=-\infty}^{\infty} I_{N_0} \mathcal{L}(\omega - W_0 - N_0\Omega_R), \quad (5)$$

This 1D spectrum be mapped into the TOP spectrum by first defining

$$\omega = \omega_1' \quad \text{for all } N',$$

where N' is an integer, as shown in Fig. 2B, to become

$$S(\omega_1', N') = \sum_{N_0=-\infty}^{\infty} I_{N_0}\mathcal{L}(\omega_1' - W_0 - N_0\Omega_R).$$

Then, a shearing transformation

$$\begin{pmatrix}\omega_1\\ N\end{pmatrix} = \begin{pmatrix}1 & \Omega_R\\ 0 & 1\end{pmatrix}\begin{pmatrix}\omega_1'\\ N'\end{pmatrix}$$

is applied to move the signal into a coordinate system where

$$S(\omega_1, N) = \sum_{N_0=-\infty}^{\infty} I_{N_0}\mathcal{L}(\omega_1 - W_0 - (N_0 - N)\Omega_R),$$

as shown in Fig. 2C. Finally, since

$$\mathcal{L}(\omega_1 - W_0 - (N_0 - N)\Omega_R) = \mathcal{L}(\omega_1 - W_0)\delta(N_0 - N)$$

we obtain

$$S(\omega_1, N) = I_N\mathcal{L}(\omega_1 - W_0).$$

We found the TOP spectrum more easily constructed using the frequency domain approach with the conventional 1D spectrum, after it has been phase corrected and any baseline roll removed. Subspectra can be extracted with arbitrary spectral width (vide infra), although Ω_R is typically used.

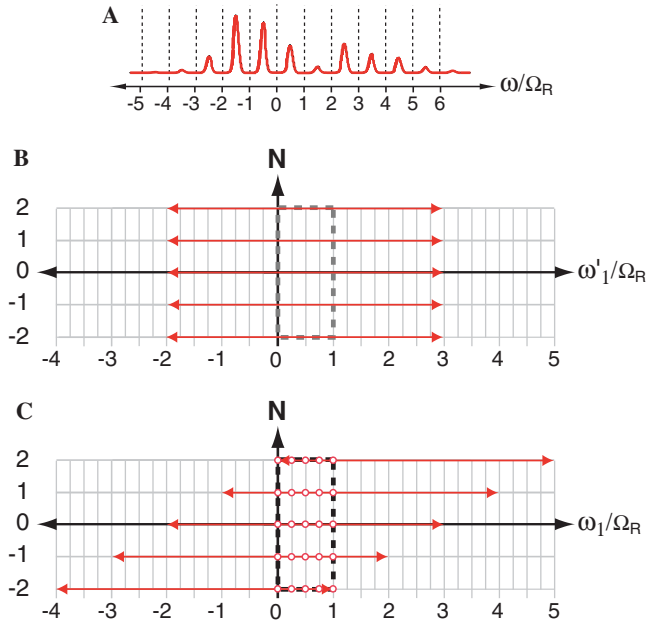

Fig. 2. (A) One pulse sample spinning spectrum. (B) Mapping of 1D spectrum into 2D $\omega_1' - N'$ coordinate system. Identical data sets are aligned and parallel. (C) 2D spectrum in ω_1–N coordinate system, which correlates frequency to sideband order, after shearing transformation of 2D spectrum in (B).

The spinning rate can often be measured more accurately from the sideband spacing in the 1D spectrum. Errors in the Ω_R used in the TOP processing are easily detected and corrected since they will result in skewed sideband patterns in the TOP spectrum. Interpolation inside the 1D spectrum when extracting subspectra is used to eliminate acquisition timing constraints. The TOP processing is freely available in the NMR data processing software package "dm-fit" [9]. Because satellite transitions are detected in TOP, the magic-angle must be set with same level of accuracy needed for STMAS [10]. In practice, we found the TOP spectrum, itself, provides a straightforward approach for using the satellite transition lineshapes to set the magic-angle.

3. Discussion

Fig. 3 shows the ^{27}Al TOP spectrum of YAG: $Y_3Al_5O_{12}$ constructed by stacking subspectra of spectral width Ω_R from its MAS spectrum. YAG has two aluminum sites, AlO_4 and AlO_6, with axially symmetric quadrupolar couplings of 6.07 and 0.6 MHz, respectively [11]. These sites are easily distinguished in the TOP spectrum, with the AlO_4 resonance spanning a wider sideband order range than the AlO_6 resonance, as expected. The sideband intensity pattern for each site can be separated with a partial projection onto the sideband order dimension and analyzed for the anisotropy tensor parameters. The large quadrupolar coupling of AlO_4 results in its central and satellite transitions being separated and shifted by the second-order quadrupolar interaction.

The inner satellite $\langle\pm3/2, \pm1/2\rangle$ transition pair occurs to the left of the central transition $\langle\pm1/2\rangle$, while the outer

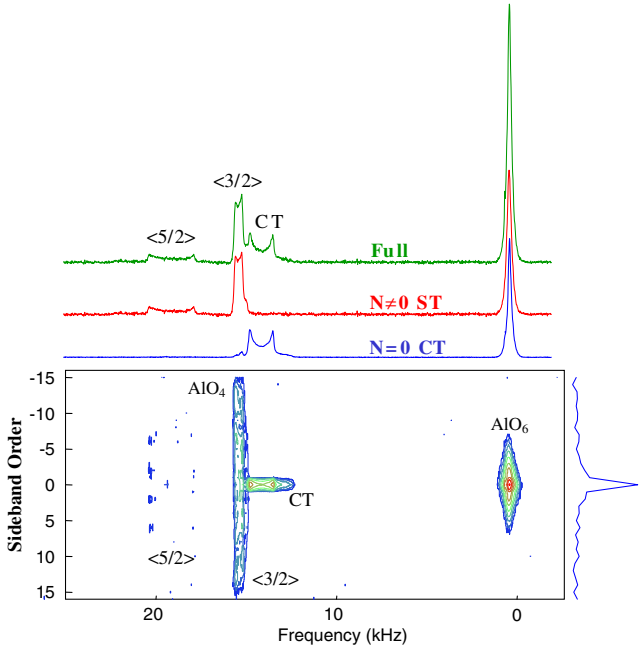

Fig. 3. ^{27}Al TOP spectrum with projections of YAG ($Y_3Al_5O_{12}$) acquired at 17.6 T while spinning at 31,250 Hz (1 MHz spectral width, 1 μs pulse ≈π/6, 5 s recycle time, 128 scans).

satellite $\langle \pm 5/2, \pm 3/2 \rangle$ transition pair is shifted furthest left and lower in intensity. In contrast, since the AlO_6 resonance has negligible second-order effects there are no shifts in the center of gravity for each of its transitions. This results in all its spinning sidebands being lined up with the $N = 0$ (i.e., central transition) component. Also in Fig. 3 are the partial and full projections onto the frequency dimension. In the $N = 0$ cross-section the central transitions for the AlO_4 and AlO_6 sites dominate. Contributions from the satellite transitions in the $N = 0$ cross-section are generally weaker, although they are higher for the AlO_6 site, due to its small quadrupolar coupling, and thus care should be taken if a quantitative analysis of the spectrum is performed [11]. The full projection, equivalent to the synchronous acquisition spectrum [12] shows all the transitions, and the projection over cross-sections with $N \neq 0$ contains only the satellite transitions (minus the intensity of the $N = 0$ band). Note that the full projection has a substantially lower signal-to-noise ratio than the $N = 0$ cross-section.

Also note in Fig. 3 that the linewidth of the inner satellite transition is narrower than the outer satellite and central transition. This well-known narrowing [13–15], summarized in Table 1, can be readily exploited with TOP. For spin $I = 5/2$ it is the inner satellite pair which are the narrowest, whereas for spins $I = 7/2$ and 9/2 it is the 2nd inner satellite pair, $\langle \pm 5/2, \pm 3/2 \rangle$. In Fig. 4 is the TOP spectrum at 17.6 T of A9B2 ($9Al_2O_3$ $2B_2O_3$), a crystalline compound with four different Al sites [15]. Although the four sites are not resolved in the $N = 0$ cross-section (central transitions), the projection over the inner satellite transition ($N \neq 0$) has much better resolution and compares well with the central transition spectrum obtained at ultra high field (40 T) [16]. Such an approach could also be useful for detecting third-order quadrupolar [17] or quadrupolar CSA cross terms [18] which only affect the satellite transitions.

In Fig. 5 is another example of an ^{27}Al MAS spectrum of a calcium alumino-silicate glass of hyper aluminous composition (50% SiO_2, 40% Al_2O_3, and 10% CaO) which exhibits overlapping contributions of AlO_4, AlO_5, and

Table 1
Scaling factors for second-order isotropic shifts: cg, $= I(I+1)$ $-9m(m-1)$ -3, and second-order anisotropy: br $= 6I(I+1)$ $-34m(m-1)$ -13

Transition		$I = 3/2$	$I = 5/2$	$I = 7/2$	$I = 9/2$
1/2	cg	3	8	15	24
	br	18	48	90	144
3/2	cg	−6	−1	6	15
	br	−16	14	56	110
5/2	cg		−28	−21	−12
	br		−88	−46	8
7/2	cg			−66	−57
	br			−216	−162
9/2	cg				−120
	br				−400

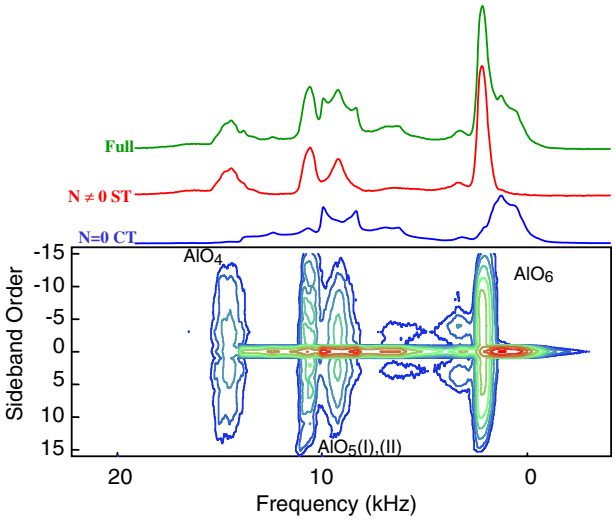

Fig. 4. ^{27}Al TOP spectrum, and projections of A_9B_2 ($9Al_2O_3$–$2B_2O_3$) acquired at 17.6 T with $\Omega_R/2\pi = 31{,}248$ Hz (1 MHz spectral width, 1 μs pulse ≈ π/6, 1 s recycle time, 300 scans).

AlO_6 environments. In previous MQMAS and MAS experiments [15] the different sites could be resolved and quantified. In the satellite transition projection of the TOP spectrum they are also clearly resolved. Moreover, because the second-order anisotropy is significantly reduced on the inner satellite $\langle \pm 3/2, \pm 1/2 \rangle$ ST_1 transitions, most of their linewidth is due to the distribution of chemical shift that can be measured by fitting the spectrum.

Although subspectra must be shifted by integer multiples of Ω_R when constructing the TOP spectrum, the subspectral width need not be Ω_R. A wider sub-spectral width can be useful to eliminate centerband aliasing. Unfortunately, this introduces additional bands into the frequency dimension, so centerbands need to be distinguished from sidebands. Generally, a center of gravity calculation along the sideband order dimension will identify an unaliased centerband, since its center of gravity will lie in the $N = 0$ cross-section. Such a calculation, however, is unnecessary for half-integer quadrupolar nuclei with strong couplings, since centerbands can readily be identified by an intense central transition resonance in the $N = 0$ cross-section. This approach can even be adopted when chemical shift anisotropy is dominant, provided Ω_R is sufficiently fast that the centerband is most intense. For example, in Fig. 6 is the ^{17}O TOP spectrum of a Titanium oxocluster [19] Ti_{16}:$Ti_{16}O_{16}(OEt)_{32}$ constructed with a subspectral width of $1.76\Omega_R$. Six oxygen ($1\mu_2$, $3\mu_3$, and $2\mu_4$) are resolved in the frequency dimension of the TOP spectrum and their centerbands identified as the resonances with maximum intensities in the $N = 0$ cross-section. The remaining resonances (shown in gray) are sidebands.

4. Conclusions

We have demonstrated here that the TOP experiment, originally proposed by Blümich and co-workers [2,3], has

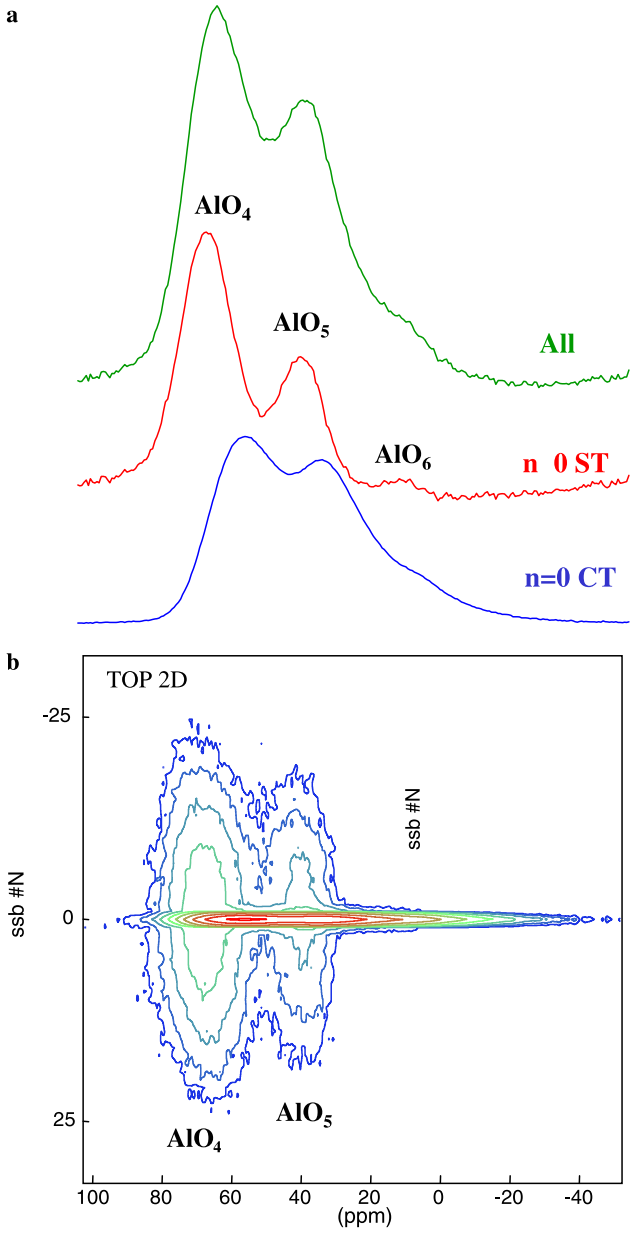

Fig. 5. (a) ^{27}Al 1D one pulse MAS, (b) TOP spectrum. Projections of a 50% SiO_2–40% Al_2O_3–10% CaO glass [15] acquired at 17.6 T while spinning at 31,258 Hz (1 MHz spectral width, 1 μs pulse ≈ π/6 1 s recycle time 40 scans). The $N = 0$ cross-section shows the central transition spectrum and the $N \neq 0$ sum is the satellite transition spectrum showing enhanced resolution with the ⟨3/2⟩ transitions mostly broadened by the distribution of isotropic chemical shift.

a number of added advantages when applied to half-integer quadrupolar nuclei. The main strength of this new approach for presenting MAS data of half-integer quadrupolar nuclei lies in its rapid interpretation. The simplicity in performing the TOP rearrangement makes it quite compelling, generally applicable, and potentially, of interest to a wide range of scientists in materials chemistry using solid-state NMR. Additionally, the ability of the TOP approach to reconstruct the higher resolution satellite transition spectrum in a simple one pulse experiment is a unique feature by itself.

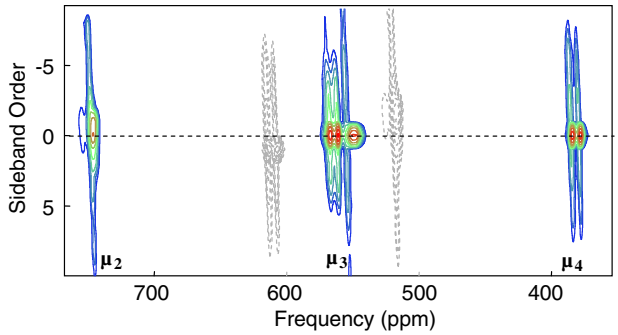

Fig. 6. ^{17}O TOP spectrum of enriched $Ti_{16}O_{16}(OEt)_{32}$ acquired at 9.4 T with $\Omega_R/2\pi = 12{,}449$ Hz (500 kHz spectral width, 2 μs pulse ≈ π/6, 1 s recycle time, 8192 scans).

We have also presented a general theoretical framework in which the data processing for TOP, as well, as MAT and PASS can be viewed. The 1D to 2D mapping of TOP can also be extended to any direct or indirect dimension having spinning sidebands. Further work investigating such possibilities for half-integer quadrupolar nuclei is warranted.

Acknowledgments

We acknowledge financial support from CNRS UPR4212, Region Centre, FNADT, and Ministere de la Recherche. P.J.G. acknowledges Le Studium, and the National Science Foundation (CHE 0111109).

References

[1] J. Herzfeld, A.E. Berger, Sideband intensities in NMR spectra of samples spinning at the magic angle, J. Chem. Phys. 73 (1980) 6021.
[2] B. Blümich, P. Blumler, J. Jansen, Presentation of sideband envelopes by two-dimensional one-pulse (TOP) spectroscopy, Solid State NMR 1 (1992) 111–113.
[3] P. Blumler, B. Blümich, J. Jansen, Two-dimensional one-pulse rotational echo spectra, Solid State NMR 3 (1994) 237–240.
[4] J.H. Kristensen, J.H. Bildsøe, H. Jakobsen, N.C. Nielsen, Separation of ^{2}H MAS NMR spectra by two-dimensional spectroscopy, J. Magn. Reson. 139 (1999) 314–333.
[5] W.T. Dixon, Spinning-sideband-free and spinning-sideband-only NMR spectra in spinning samples, J. Chem. Phys. 77 (1982) 1800.
[6] M. MehringHigh Resolution NMR Spectroscopy in Solids, vol. 11, Springer-Verlag, Berlin, 1983.
[7] O.N. Antzutkin, S.C. Shekar, M.H. Levitt, Two-dimensional sideband separation in magic-angle spinning NMR, J. Magn. Reson. A 115 (1995) 7–19.
[8] D.W. Alderman, G. McGeorge, J.Z. Hu, R.J. Pugmire, D.M. Grant, A sensitive, high resolution magic-angle turning experiment for measuring chemical shift tensor principal values, Mol. Phys. 95 (6) (1998) 1113–1126.
[9] D. Massiot, F. Fayon, M. Capron, I. King, S. Le Calv, B. Alonso, J.-O. Durand, B. Bujoli, Z. Gan, G. Hoatson, Modelling one and two-dimensional solid-state NMR spectra, Magn. Reson. Chem. 40 (2002) 70–76.
[10] Z. Gan, Isotropic NMR spectra of half-integer quadrupolar nuclei using satellite transitions and magic-angle spinning, J. Am. Chem. Soc. 122 (2000) 3242–3243.
[11] D. Massiot, C. Bessada, J.P. Coutures, F. Taulelle, A quantitative study of aluminum-27 MAS NMR in crystalline YAG, J. Magn. Reson. 90 (1990) 231–242.

[12] S.E. Ashbrook, S. Wimperis, Rotor-synchronized acquisition of quadrupolar satellite-transition NMR spectra: practical aspects and double-quantum filtration, J. Magn. Reson. 177 (2005) 44–55.
[13] A. Samoson, Satellite transition high-resolution NMR of quadrupolar nuclei in powders, Chem. Phys. Lett. 119 (1985) 29–32.
[14] C. Jäger, How to get more from ^{27}Al MAS NMR by high-speed satellite-transition spectroscopy, J. Magn. Reson. 92 (1992) 353–362.
[15] D. Massiot, D. Miiller, Th. Hubert, M. Schneider, A.P.M. Kentgens, B. Cote, J.P. Coutures, W. Gessner, DOR and MAS NMR study of ^{27}Al : Reexamination of the aluminum borate 9 Al_2O_3–2 B_2O_3, Solid State NMR 5 (1995) 175–180.
[16] Z.H. Gan, P. Gor'kov, T.A. Cross, A. Samoson, D. Massiot, Seeking higher resolution and sensitivity for NMR of quadrupolar nuclei at ultrahigh magnetic fields, J. Am. Chem. Soc. 124 (2002) 5634–5645.
[17] Zhehong Gan, Parthasarathy Srinivasan, John R. Quine, Stefan Steuernagel, Bennoc Knott, Third-order effect in solid-state NMR of quadrupolar nuclei, Chem. Phys. Lett. 367 (1–2) (2003) 163–169.
[18] S. Wi, S.E. Ashbrook, S. Wimperis, L. Frydman, Second-order quadrupole-shielding effects in magic-angle spinning solid-state nuclear magnetic resonance, J. Chem. Phys. 118 (7) (2003) 3131–3140.
[19] E. Scolan, C. Magnenet, D. Massiot, C. Sanchez, Surface and bulk characterisation of titanium oxo clusters and nanosized titania particles through ^{17}O solid state NMR, J. Mater. Chem. 9 (1999) 2467–2474.